The Astrophysical Journal, 776:109 (13pp), 2013 October 20 doi:10.1088/0004-637X/776/2/109

THE SOLAR WIND AS A POSSIBLE SOURCE OF FAST TEMPORAL VARIATIONS OF THE HELIOSPHERIC RIBBON

H. Kucharek[1], S. A. Fuselier[2,3], P. Wurz[4], N. Pogorelov[5], S. Borovikov[5], M. A. Lee[1], E. Moebius[1], D. Reisenfeld[6], H. Funsten[7], N. Schwadron[1], and D. McComas[2,3]
[1] Space Science Center, University of New Hampshire, Durham, NH, USA; harald.kucharek@unh.edu
[2] Southwest Research Institute, San Antonio, TX, USA
[3] Department of Physics, University of Texas at San Antonio, San Antonio, TX, USA
[4] Physikalisches Institut der Universitaet Bern, Bern, Switzerland
[5] Physics Department and Center of Space Plasma and Aeronomic Research, The University of Alabama, Huntsville, AL, USA
[6] Department of Physics and Astronomy, University of Montana, Missoula, MT, USA
[7] Center of Space Science and Exploration, Los Alamos National Laboratory, Los Alamos, NM, USA
Received 2012 December 28; accepted 2013 July 18; published 2013 October 4

ABSTRACT

We present a possible source of pickup ions (PUIs) the ribbon observed by the *Interstellar Boundary EXplorer* (*IBEX*). We suggest that a gyrating solar wind and PUIs in the ramp and in the near downstream region of the termination shock (TS) could provide a significant source of energetic neutral atoms (ENAs) in the ribbon. A fraction of the solar wind and PUIs are reflected and energized during the first contact with the TS. Some of the solar wind may be reflected propagating toward the Sun but most of the solar wind ions form a gyrating beam-like distribution that persists until it is fully thermalized further downstream. Depending on the strength of the shock, these gyrating distributions can exist for many gyration periods until they are scattered/thermalized due to wave–particle interactions at the TS and downstream in the heliosheath. During this time, ENAs can be produced by charge exchange of interstellar neutral atoms with the gyrating ions. In order to determine the flux of energetic ions, we estimate the solar wind flux at the TS using pressure estimates inferred from in situ measurements. Assuming an average path length in the radial direction of the order of a few AU before the distribution of gyrating ions is thermalized, one can explain a significant fraction of the intensity of ENAs in the ribbon observed by *IBEX*. With a localized source and such a short integration path, this model would also allow fast time variations of the ENA flux.

Key words: ISM: atoms – ISM: magnetic fields – shock waves – solar wind

Online-only material: color figures

1. INTRODUCTION

The *Interstellar Boundary EXplorer* (*IBEX*), launched in 2008 October, is the first mission that was designed to image the heliosphere in the light of energetic neutral atoms (ENAs; McComas et al. 2009a). The IBEX payload consisted of two sensors, *IBEX-lo* (Fuselier et al. 2009) and *IBEX-hi* (Funsten et al. 2009a), covering an energy range of 0.01–6 keV nucleon^{-1}. In mid-2009, *IBEX* finished its first full sky scan and returned the first sky maps of ENAs. The sky maps revealed a large-scale structure that was completely unexpected and not predicted by any of the models that existed prior to launch (McComas et al. 2009b). Since then, this structure, called the ribbon, has been under intensive investigation. A number of models have been proposed to explain the formation, source, and location of this ribbon. A summary of these ideas can be found in McComas et al. (2009b, 2010). Recently, Heerikhuisen et al. (2010) followed up on one of these ideas with a numerical model that relies on the neutral component of the solar wind that penetrates into the interstellar medium. In the interstellar medium, hydrogen atoms generate a pickup ion (PUI) population by charge exchange. These PUIs then experience another charge exchange, leading to so-called secondary ENAs. According to this model, secondary ENAs are the source population for the ribbon. However, in order to reproduce the ENA intensity measured in the ribbon, a relatively long line of sight path length is required that ranges up to several tens of AU. Furthermore, this approach may require relatively stable ring-beam distributions over several years. These distributions, however, are subject to instabilities and it is still under intensive debate how long these ion ring distributions can last under these plasma conditions (Gamayunov et al. 2010, 2012). If one assumes stable PUI distributions without wave–particle interactions, then one would obtain a relatively thin ribbon. Chalov et al. (2010) provided another model that includes secondary charge exchange of the interstellar H atoms with the interstellar pickup protons (PUPs) outside the heliopause (HP). In contrast with the previously described model, these authors solve consistently for the motion of PUPs along magnetic field lines in the scatter-free limit and thus include the motion of PUIs along the field line between their pickup and re-neutralization. Both models assume that ENAs are produced beyond the termination shock (TS) outside the HP. Furthermore, the region in which ENAs are generated needs to be several 100 AU to reproduce the measured ENA flux observed by *IBEX*. The largest contribution to the ENA intensity, however, is within the first 50 AU (Heerikhuisen & Pogorelov 2011).

In this paper, we propose a different approach. Here, we introduce a model that could account for the relatively fast temporal and spatial changes of the ENA flux. We divide the ENA flux into a static (or less variable) component and a variable component. The variable component is superimposed on a static ENA flux and is responsible for the fast temporal changes that may occur in the ribbon. Unlike the previous models that assume a distant source and a wide ENA production region, we suggest that the reflected solar wind (including PUIs) at the TS and in

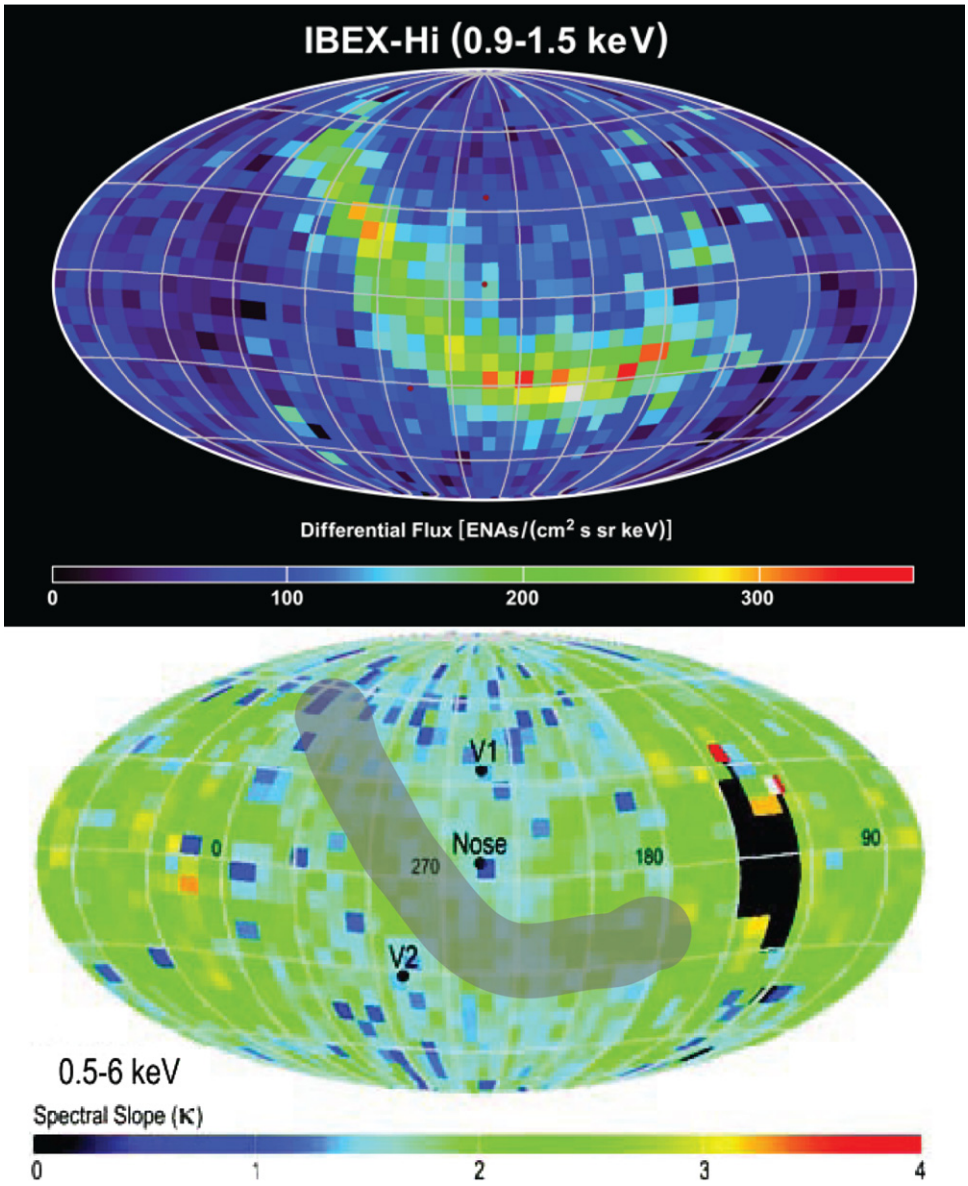

Figure 1. Top: the heliospheric ribbon, as observed by *IBEX-hi* in the energy range of 1.1 keV. The gray shaded area marks the average location of the ribbon in an angular range of $\pm 20^{\circ}$. Bottom: sky map of the spectral slope, as observed by *IBEX-lo* and *IBEX-hi* in the energy range 0.5–6 keV. The gray shaded area marks the location of the ribbon.

the immediate downstream region could be a powerful source of ENA production. Since we assume that the ENA source (the ENA creation region) is relatively near (ribbon at 84 AU) and localized (of the order of AU thick), this model could account for any fast temporal (and spatial) changes in the ENA maps (McComas et al. 2009a, 2009b, 2010). We also propose that the ribbon may be associated with the global geometry of the TS, which may be shaped by the interstellar magnetic field. In the framework of this model, one could generate a ribbon that is on average uniform but could contain relatively fast ENA flux variations.

We organize this paper as follows. In the first part of this paper, we revisit the most recent *IBEX* results and the properties of the observed *IBEX* ribbon. We combine those observations with *Voyager 1* (V1) and *Voyager 2* (V2) measurements when they are near the TS. Based on these observational results, we identify a possible source and a possible formation mechanism. We then discuss the source location and intensity and compare the estimated ENA flux with *IBEX* current observations. In this section, we also present numerical simulations that support the basic idea of the ENA generation mechanism. We then discuss the role of the interstellar magnetic field and the formation and shape of the *IBEX* ribbon and its association with the global shape of the TS. Global magneto hydrodynamic (MHD) simulations are presented to provide evidence for our simplified assumptions of the shape of the TS. In the last section of this paper, we summarize our findings, discuss uncertainties and unknowns, and provide predictions for possible future ribbon variations.

1.1. Properties of the IBEX Ribbon

McComas et al. (2009a, 2009b), Fuselier et al. (2009), Funsten et al. 2009b, and Schwadron et al. (2009) describe the discovery of the ribbon-like feature in light of ENAs. This ribbon structure is on average 20° wide (FWHM) and seems to be aligned with a region in which the radial vector $\mathbf{R}$ is perpendicular to the interstellar magnetic field $\mathbf{B}$ ($\mathbf{R} \cdot \mathbf{B} = \mathbf{0}$), draped around the HP (see Figure 1, top panel). The gray shaded area in

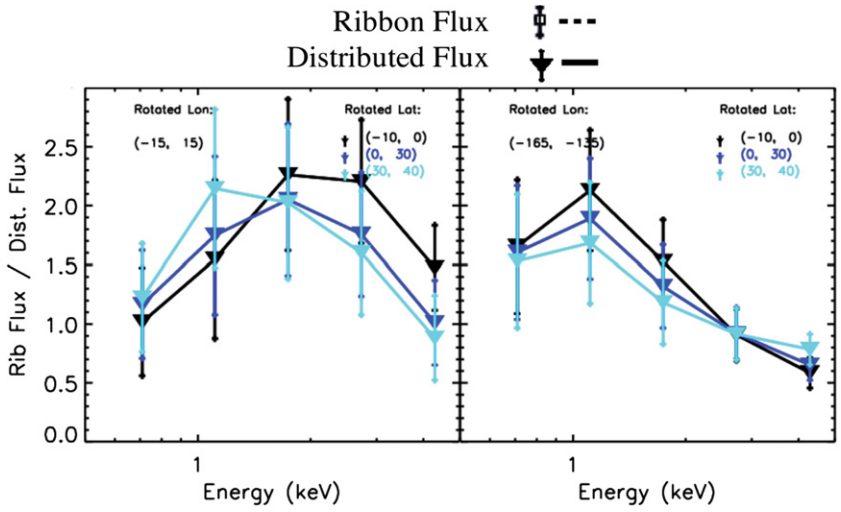

Figure 2. Intensity of the ribbon integrated along the $R \cdot B = 0$ line as a function of energy. Both energy ranges of *IBEX-lo* and *IBEX-hi* have been combined.

Figure 1 shows the approximate location of the ribbon feature. Fuselier et al. (2009) found that the angular width of the ribbon appears to increase with increasing energy. However, if one subtracts the distributed flux, the width of the ribbon does not change with energy. This fact, of course, raises questions about the source of the ribbon and the distributed ENA flux around the ribbon. More details of the properties of the ribbon and the distributed flux can be found in Schwadron et al. (2011). The orientation of this ribbon seems to be nearly perpendicular to the model-predicted interstellar field (Heerikhuisen et al. 2010). Furthermore, the first set of *IBEX* sky maps revealed that this ribbon is not uniform in intensity. High ENA intensities are observed in relatively localized regions. Some of these regions are at higher ecliptic latitudes and could be associated with the high-speed solar wind. There is also an indication of a bifurcated signature of ENA emission closer to the ecliptic plane. A sky map containing the slopes of energy spectra from 0.2 to 4.2 keV in each $6^\circ \times 6^\circ$ pixel has been composed (see Figure 1, bottom panel). In this representation, the ribbon (indicated by the gray shaded area) is not visible or, in other words, there is no contrast with the surrounding regions. There are, however, significant differences closer to the tail regions. The absence of the ribbon in this slope map provides good evidence that sources and physical processes producing the ENA emission in the surrounding and in the location of the ribbon are not significantly different and are most likely the same. An intensity enhancement in the ENA emission can be achieved by locally increasing the density of the source population without engaging other acceleration processes. Fuselier et al. (2009), as well as Schwadron et al. (2011), reported that the ENA intensity is a function of energy. Over the energy range of *IBEX-hi* and *IBEX-lo*, the ribbon intensity peaks at 1.1 keV and decreases rapidly toward higher and lower energies (see Figure 2; after Schwadron et al. 2011). Clearly, the peak energy is on the order of that of the solar wind observed by V1 and V2 before the spacecraft crossed the TS. The measured bulk speed was around 380 km s^{-1}, which corresponds to ~1 keV (Decker et al. 2005; Burlaga et al. 2005). A gyrating solar wind gas in the shock ramp and in the near downstream region would have approximately the same energy as the solar wind entering the shock. An ENA created by charge exchange of interstellar neutrals with these gyrating solar wind ions would be in the energy range of the observed ENA peak energy. In a recent paper, McComas et al. (2012) presented a study of 3 yr of ENA observations and the evolution of the ENA maps and the ribbon. Their results also provided strong indication of a quite direct and latitude-dependent solar wind source of the ribbon.

2. *VOYAGER* OBSERVATIONS IN THE NEIGHBORHOOD OF THE *IBEX* RIBBON AND THE ROLE OF THE INTERSTELLAR MAGNETIC FIELD

Although the V1 and V2 spacecrafts missed the ribbon structure, they do provide in situ measurements within several tens of degrees of this structure. V1 crossed the TS on 2004 December 16 north of the ribbon (Stone et al. 2005). About 2 yr before the crossing, beams of precursor ions propagating along the interplanetary magnetic field toward the spacecraft were observed. A similar pattern was seen by V2, which also observed similar streaming precursor ions as it approached the TS. However, the distance of the TS from the Sun was different: 94 AU for V1 and 84 AU for V2. Ratkiewicz et al. (2000) and Izmodenov et al. (2005) investigated the impact of the interstellar magnetic field on the location and shape of the TS. They found that the TS and the HP are displaced by several AU toward the Sun based on the effect of the interstellar magnetic field ($B_{\rm LIC} = 2.5\,\mu$G). Using global MHD simulations, Pogorelov & Matsuda (1998) and Ratkiewicz et al. (1998) showed that the interstellar magnetic field produces a north-south asymmetry of the HP and the TS. Opher et al. (2006) and Jokipii et al. (2007) used this asymmetry to explain energetic particle observations. They argued that this asymmetry of the shock may cause several encounters of the interplanetary magnetic field (Parker spiral) with the shock surface. High energy particles could then be streaming toward the Sun along the spiral interplanetary magnetic field connecting V1 and the shock. These simulations also indicated that the shock and the HP in the upwind direction are closer to the Sun in the direction where the radial vector is perpendicular to $B_{\rm LIC}$. The distance of the Sun to the TS is smallest compared with the distances in all other directions. Since an isotropic ENA source decreases with $1/R^2$, where R is the heliocentric distance, the ENA signal from this region would be most intense if the neutrals originating from this area reached the *IBEX* detectors. Ratkiewicz et al. (2012) showed the effects of the strength and direction of the local interstellar magnetic field on the heliospheric geometry.

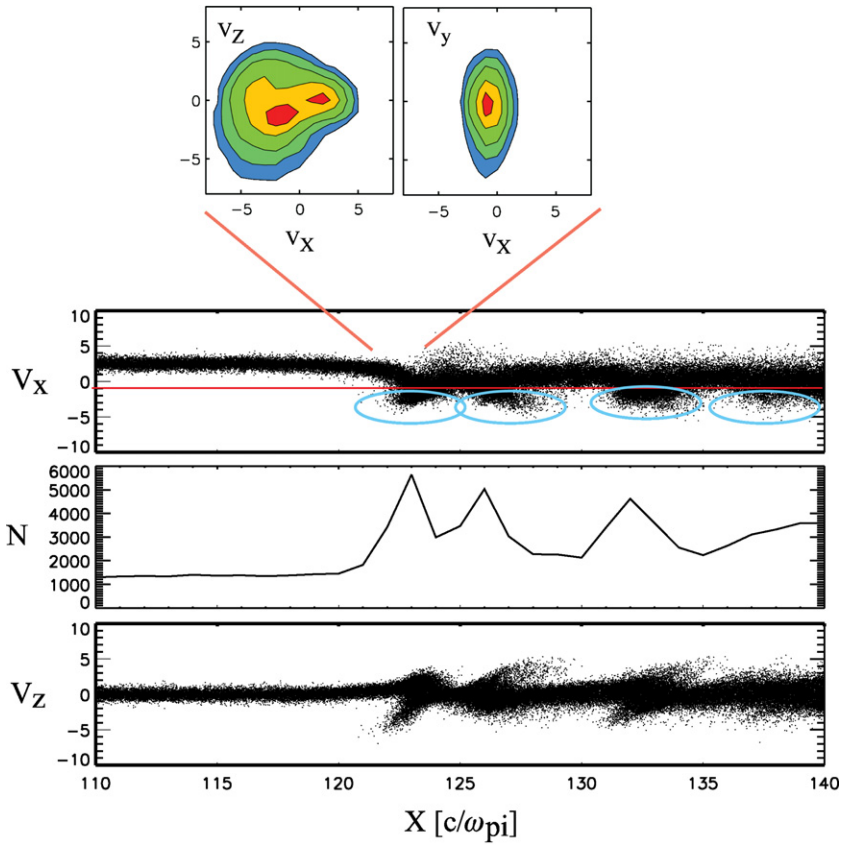

Figure 3. Phase space plots from a 2D hybrid simulation. The top two panels show V_x, the middle panel shows the number of solar wind ions per ion inertial length, and the bottom panel shows and V_z along X. For this plot, we show the phase space of all ions that are in a area of only $10c/\omega_{pi}$ in the Y direction. Since the simulation is 2D, the phase space is 3D. We therefore show also the particle distribution in velocity ($V_x - V_y$ and $V_x - V_z$) space. At the shock ramp, we shock more details (see insert) of the phase space. We show the $V_x - V_y$ and $V_x - V_z$ velocity space distribution. The red contours mark the 75% level relative to the maximum intensity. These cuts in velocity phase space indicate a relatively narrow ring distribution. The light blue circles shown on the $V_x - X$ plot mark areas downstream of the shock in which one finds similar distributions.

This geometry then generates a locus of points associated with the position of the *IBEX* ribbon. Ratkiewicz et al. (2012) also confirmed and supported the existence of a strong physical relationship between the ribbon and the interstellar magnetic field. As we will show below, the interstellar magnetic field may affect the global geometry of the TS and thus the formation of the ribbon. Although the *Voyager* spacecraft did not enter the TS at the location of the ribbon structure, these measurements provide very important information on the microphysics that occurs close to the TS, which we will discuss in the next two subsections.

2.1. Local Dynamics of the TS and the Gyrating Ion Populations

The *Voyager* spacecraft returned very useful information on the strength and dynamics of the TS as they crossed that region of space. Burlaga et al. (2005) determined the Mach number ($M_A \sim 4$) and shock properties, which indicate a perpendicular shock. These authors point out that the shock was reforming. Shock reformation is a known feature that was predicted by numerical simulations (Burgess et al. 1989) and confirmed by Cluster observations (Moullard et al. 2006) for the perpendicular Earth's bow shock. Two years before the *Voyager* spacecraft crossed the TS, they reported energetic Sun-ward streaming ions. These ions, which are likely ion beams, are also a feature of a quasi-perpendicular shock.

Burgess & Scholer (2007) performed multi-dimensional hybrid simulations and confirmed that the local shock structure is determined by gyrating ion populations. This fact indicates that the local shock structure and the process of shock reformation and energetic ion beams upstream of a quasi-perpendicular shock are closely associated with a gyrating ion population. This population could be a strong source of ENA production because it is gyrating perpendicular to the magnetic field as a cold ring beam-like distribution and therefore these ions have a large perpendicular velocity. These gyrating ring distributions are unstable and can most likely be found near the shock and in the downstream region until they are thermalized downstream by wave–particle interactions. Depending on the shock strength, this process may take numerous ion gyrations for a marginally supercritical shock (Liu et al. 2007).

In the following subsections, we pursue the idea that these ring distributions could be a strong source of ENAs. In order to demonstrate the possibility of ring beam-like ion distributions at the quasi-perpendicular shock, we performed two-dimensional (2D) multi-species hybrid simulations in which we self-consistently included solar wind protons, solar wind helium, PUPs, and hydrogen neutrals. We then estimated the intensity of ENAs produced by these distributions.

2.2. Evidence for a Gyrating Solar Wind from Numerical Simulations

Figure 3 shows the results of a 2D multi-species hybrid simulation for a (quasi-) perpendicular shock ($\theta_{BN} = 80^\circ$). In these simulations, ions are treated as macro particles and the equations of motion are solved while electrons are treated as

a charge-neutralizing fluid. Solar wind protons and PUIs are treated self-consistently. All velocities in these simulations are normalized to the Alfvén speed and the length is measured in ion inertial lengths (c/ω_{pi}), where c is the speed of light and ω_{pi} is the proton plasma frequency. The solar wind is injected from the left side and reflected on the right side by a conducting wall. Due to the interaction of the incoming solar wind and the reflected ions, a shock is launched propagating from the right to the left. In this simulation, the shock ramp is located around $123(c/\omega_{pi})$. For the analysis of the distributions, we limited our coordinate space in the y-direction to $10c/\Omega_{pi}$. In Figure 3, we show the solar wind phase space $V_x - X$ (top panel), $V_z - X$ (bottom panel), and the density of the core solar wind N. As one can see in the $V_x - X$ presentation, almost the entire distribution of incoming solar wind protons goes through the shock ramp, starts gyrating at the shock front, and forms a ring beam-like distribution. This result is also supported by the proton distribution in velocity space ($V_x - V_y$ and $V_x - V_z$) inside the shock ramp. The red contours (75% level) indicate a ring distribution that rotates perpendicular to the mean local magnetic field. The red line in the $V_x - X$ panel indicates the shock ramp speed and thus it separates the ions in velocity space propagating upstream or downstream at this instance in time. The gyration of that population continues downstream for several gyro-periods until the plasma is fully thermalized. The light blue circles mark areas in the phase space at which the bulk speed is negative and larger than the shock speed. ENAs generated by these distributions could propagate inward toward the Sun and could be detected by *IBEX*. The density of the core solar wind reveals that the downstream density compression is a factor of three with large density fluctuations. These fluctuations can reach a factor of five in the overshoot region of the shock. These fluctuations become smaller when the wave–particle scattering destroys the ring distributions and the plasma is more and more thermalized downstream. The PUI distribution is not shown. These ions are suprathermal and provide a major fraction of the downstream thermalization at such a high abundance. Solar wind ions become more and more like test particles at the shock as the PUI abundance increases.

2.3. Contribution of Solar Wind Protons and Pickup Ions

In the previous subsection, we only considered solar wind protons. However, the TS is a PUI mediated shock because the PUI content in the solar wind is relatively high at 100 AU. Unfortunately, there are no direct measurements of PUIs at energies around 1 keV at the TS. The energy range of *Voyager* particle instruments starts at around 10–20 keV (Krimigis et al. 1977). One can estimate the number density ratio of PUIs to solar wind ions. The density of solar wind ions decreases with increasing heliospheric distance as $n_{\rm sw} = 1/R^2$ (radial expansion), whereas the pickup density decreases as $n_{\rm pui} = 1/R$ for a perpendicular magnetic field. Therefore, the ratio of $n_{\rm sw}/n_{\rm pui}$ is proportional to R^{-1}. At the TS, we can calculate that this ratio is of the order of $n_{\rm pui}/n_{\rm sw} = 0.2$–$0.3$. Another important factor for ENA production is the phase space distribution at the location where the charge exchange occurs. Observations show that upstream of the shock, the solar wind protons show a kappa-like distribution function that is confined in velocity space and peaks at the solar wind bulk speed. Usually, the solar wind distribution is approximated by a Maxwellian distribution. Upstream of the shock and in the solar wind frame, the phase space distribution of PUIs is a filled-shell distribution with a radius of the solar wind speed and centered around the solar wind bulk speed (Vasyliunas & Siscoe 1976). At the shock and downstream of the shock, these distributions will be mediated by wave–particle interactions and will form a combined ion distribution. Hence, after charge exchange, the ENA distribution represents a copy of the charged ion distribution; an ion beam distribution would favor ENA production in a specific direction. Furthermore, since the pickup distribution is broader in velocity space, it will not peak at 1 keV and the total peak intensity will be lower. A contribution to the ENA flux from charge exchange with PUIs cannot be excluded and a significant fraction of the observed ENAs may actually be created by the charge exchange of interstellar neutrals with PUIs.

In the next subsection, we do not differentiate between solar wind ions and PUIs. However, one should keep in mind that the number density of PUIs is approximately ~30% of the solar wind protons and that their velocity phase space distributions are different. The ratio $n_{\rm pui}/n_{\rm sw}$ can have different values because fewer solar wind ions are reflected. This situation will be investigated in more detail below.

3. THE ENA FLUX PRODUCED BY GYRATING SOLAR WIND IONS

The energy of the gyrating solar wind population at lower latitudes is comparable with the peak energy of the observed ENAs in the ribbon. Therefore, we can ask if the downstream gyrating solar wind that charge exchanges with the interstellar neutrals is a significant source of the ENAs in the ribbon. How much ENA flux could be produced by reflected solar wind ions? One important factor is the form of the distribution. A ring-like distribution is more or less 2D and therefore denser in phase space than a three-dimensional (3D) shell distribution. The directional flux of ENAs created by charge exchange is given by a line of sight integral:

$$J_{s,\rm ENA}(r_0, E) = \int_0^{\lambda} J_p(s, E)\sigma(E)n_{\rm H}(s)\exp[-D(s, E)]ds, \quad (1)$$

where $J_p(s, E)$ is the directional differential flux of protons in the heliosheath with an energy E, $n_{\rm H}(s)$ is the local number density of interstellar hydrogen atoms, and $\sigma(E)$ is the energy-dependent charge exchange cross-section. The extinction factor of ENAs is given by $D(s, E) = \int(\beta p + \beta e + \beta\nu)dt$, where the βp is the loss of ENAs due to charge exchange with solar wind protons, βe describes the loss due to electron impacts, and $\beta\nu$ is the loss due to solar photoionization. The integration is performed along the path of an atom's trajectory. In the following calculation, we neglect the extinction, which is small. For the energy-dependent cross-section, we use $\sigma(E)$ from Cummings et al. (2002). These authors show that the charge exchange cross-section of an interstellar neutral hydrogen with a proton is approximately velocity independent over the range of velocities covered by the *IBEX* sensors. Since, at this point, we are only interested in providing an estimate of the ENA flux, we assume a constant number ($\sigma(E) \sim 3 \times 10^{-15}\,{\rm cm}^2$). For the local number density of interstellar hydrogen, $n_{\rm H}(s)$, we also use a commonly accepted number, $n_{\rm H}(s) = 0.06\,{\rm cm}^{-3}$. This number may vary between $n_{\rm H}(s) = 0.06$–$0.1\,{\rm cm}^{-3}$ (see Gloeckler et al. 2004). In order to reproduce the intensity of ENAs observed by *IBEX* in the ribbon, one is left with two parameters: the directional differential flux of protons $J_p(s, E)$ and the length of the integration path λ. Unfortunately, there are no direct observations of the differential proton flux $J_p(s, E)$, so

we need to estimate this quantity. This process will then allow us to calculate the integration path λ.

One way to determine the flux of the solar wind at the TS is to assume pressure balance between conditions far upstream and far downstream of the TS. The pressure downstream is given by

$$P = \frac{1}{3} \cdot m \cdot 4\pi \int_0^{2 \cdot V_{sw}} v^4 dv f_0 = \frac{4\pi}{15} m (2V_{sw})^5 f_0, \quad (2)$$

where f_0 is the downstream distribution function of the charged component assuming $f_0 = \text{const}$ within $(2 \cdot V_{sw})$. The differential ENA intensity, which is measured by *IBEX*, can be expressed by the ENA distribution function:

$$J_{ENA} = \frac{v^2}{m} \cdot f_{ENA}, \quad (3)$$

where f_{ENA} is the ENA distribution function directed Sun-ward that results from the ion distribution function through charge exchange. Taking this fact into account, we find:

$$f_{ENA} = \lambda \cdot \sigma(E) \cdot n_H \cdot f_0. \quad (4)$$

In these equations, the real unknown is λ, the path length of the line of sight integral. The pressure at the TS can be estimated using generalized Rankine–Hugoniot conditions; Roelof et al. (2010) estimated a pressure range of 0.0077 pPa (Cassini/INCA) (5–55 keV), 0.023 pPa (V2, Low Energy Charged Particle (28–3500 keV)), and 7.5 pPa (*IBEX* in the V2 pixel). More details on the above equations are presented in Appendix A.

With this set of equations and the estimated pressure range at the TS, one can determine the path length of the line of sight integral λ for the distributed ENA flux and the ribbon flux. As shown above, the ribbon ENA signal at 1 keV is about a factor of two higher than the ambient ENA flux. Based on the findings in Section 2, we also assume that the source population is the same and that the signals are superimposed. In the following section, we discuss how the distributed ENA and the ribbon flux could be generated in the framework of this model.

3.1. Distributed ENA Flux

The measured average distributed ENA flux at 1 keV is of the order of $J_{ENA} = 150/(\text{cm}^2\,\text{s}\,\text{sr}\,\text{keV})$. Using the simple relation A4 (see Appendix A), we obtain:

$$J_{ENA} = 12\lambda(\text{AU})/(\text{cm}^2\,\text{s}\,\text{sr}\,\text{keV}). \quad (5)$$

We would, depending on the pressure at the TS, need a path length of $\lambda = 12$–20 AU. These values are smaller than the thickness of the heliosheath estimated using *Voyager* data (Krimigis et al. 2011). At the flanks of the heliosheath, one may have a larger integration path and the number of generated ENAs may be higher. However, the number of ENAs that reach the IBEX detectors is reduced because at the flanks there is flow around the TS and ENAs generated in this area that may have velocity components along the flow but not in the Sun-ward direction. It is important to note that up to this point we have used pressure balance to estimate the path length λ. Pressure balance is usually established far downstream when the plasma is fully isotropic.

3.2. Ribbon Flux and Fast ENA Variations

The ENA flux inside the ribbon is roughly a factor of two more intense and it shows more structure and slightly more temporal variability than the globally distributed flux. According to the calculation in the previous subsection, one could generate the ribbon ENA flux by doubling the integral path length to 40 AU. However, this path length would not easily allow fast variations in the ENA flux nor the fine structure seen in the ribbon. However, ring distributions that can be found in the shock ramp and in the downstream region of the TS have not yet been taken into account. These distributions could be more efficient at producing ENAs and we include the relation:

$$f_{ENA} = \lambda \cdot \sigma(E) \cdot n_H \cdot f_0 \cdot \gamma, \quad (6)$$

where γ is an enhancement factor describing a more efficient/intense source that would result in the same ENA flux from a more localized area as long as the shock normal is oriented Sun-ward so that the ring distributions may produce Sun-ward ENAs. More details are given in Appendix B. A more intense source region could be a region with a higher ion density in phase space with appropriate velocities for reaching the inner heliosphere. In Appendix B, we derive an enhancement factor that describes the number density of ENAs produced perpendicular to the magnetic field by a ring distribution relative to a fully thermalized, spherical distribution; compared with a thermalized ion distribution, a ring-beam ion distribution can be significantly more efficient. A ring-beam ion distribution with an opening angle of 10° produces about 10 times more directional flux than a fully thermalized downstream distribution. With such a high efficiency, the integration length of the path integral would be of the order of 1–2 AU. These numbers are all estimates based on thermal pressure and equilibrium conditions. Thermal pressure and downstream thermalization depend on plasma conditions and shock parameters.

Parameters such as solar wind speed, plasma β, and the PUI abundance may influence the shock strength of the TS and thus the detailed downstream thermalization. How fast the plasma is isotropized also depends on wave–particle interactions. Wave–particle interactions destroy the ring distributions because as part of the thermalization process. Furthermore, the TS is highly mediated by PUIs that impact the local shock structure and the downstream thermalization process. The larger the abundance of PUIs, the larger the contribution from the PUIs because the shock is a PUI shock and solar wind ions are not efficiently heated. The kinetics of the shock are then dominated by the PUIs. All of these processes need to be investigated in more detail, which will be the subject of future investigations.

4. THE INTERSTELLAR MAGNETIC FIELD AS A GOVERNING PARAMETER

What is the role of the interstellar field? Why is the ribbon confined to an angular range of ∼20° along a line that coincides with the line for which $\mathbf{R} \cdot \mathbf{B} = \mathbf{0}$? In other words, why is the ribbon confined to the radial vector that originates from the Sun perpendicular to the predicted orientation of the interstellar magnetic field vector **B**? As global MHD simulations of Pogorelov & Matsuda (1998) and Pogorelov et al. (2004) show, the interstellar magnetic field shapes the HP and TS. The difference in magnetic pressure creates a strong asymmetry in the distance of the HP and a weaker but still pronounced asymmetry at the TS. Therefore, the measured distance at which *V1* (V2) crossed the

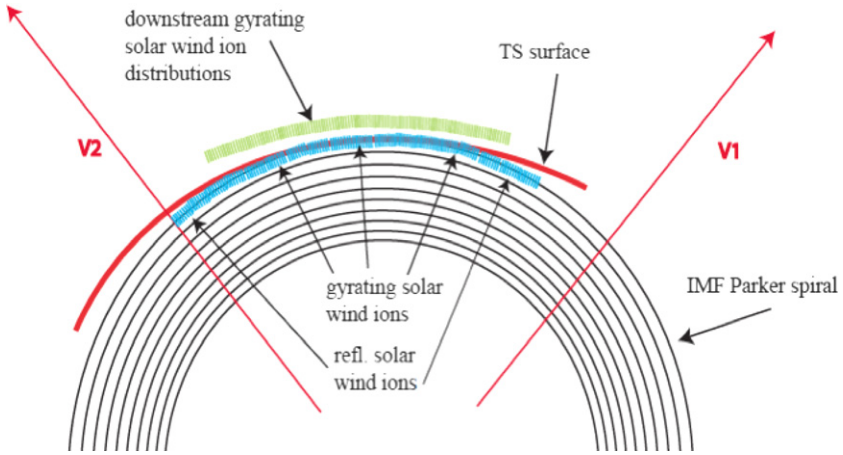

Figure 4. Schematic representation of the magnetic field topology with respect to the location of the TS. The IMF in this figure has been approximated as a Parker spiral that intersects the compressed TS twice. At those intersections, reflected ions (solar wind and PUIs) that gyrate at the shock ramp can propagate upstream (blue spirals). There is substantial evidence from global MHD simulations that the intersecting points are located between the *V1* and *V2* crossing point of the TS. A significant fraction of ions at the TS are reflected/convected until they are thermalized downstream by wave–particle interactions.

TS was 94 (84) AU. The model displacement (see Pogorelov & Matsuda 1998; Pogorelov et al. 2004) of the HP and the TS is of the order of 10 AU toward the Sun. Of course, these numbers are model numbers and depend on the assumed strength of the interstellar field. Due to the displacement of the TS and HP toward the Sun, the interplanetary magnetic field may on average intersect the surface of the TS twice (outbound and inbound) in a relatively small area (see Figure 4). Between these points, the initial mass function (IMF) orientation is parallel to the TS surface; i.e., the angle between the shock normal and the IMF (θ_{BN}) is 90°. In other words, we find ideal perpendicular shock conditions and ions will gyrate with a 90° pitch angle and will not stream along the field line while they are convected downstream of the TS. Interstellar neutrals that charge exchange with these ions will generate ENAs that have a velocity distribution that is perpendicular to the magnetic field and aligned with the shock normal direction. In all other regions that have smaller shock normal angles, ions will stream along the field line in the plasma frame. Depending on their bulk flow, ENAs generated from these ions by charge exchange will have velocities that are not radial and therefore not detected by *IBEX*. Figure 4 illustrates this situation. It should be noted that beams of energetic ions in an energy range of 40–53 keV were observed by *V1* and *V2* about 2 yr prior to the TS crossing and their bulk flow was toward the spacecraft. The two *Voyager* spacecraft crossed the TS in the direction of the ribbon but missed it on both sides. This streaming pattern could taken as an indicator of no streaming; i.e., ideal perpendicular shock conditions exist somewhere in between.

Most importantly for the model, we propose that between the entry point of *V1* and *V2* into the heliosheath, there is most likely a region at which the TS is perfectly perpendicular (disregarding possible shock ripple effects). In this region, ions gyrate with a 90° pitch angle without drifting sideways (upstream). This region is ideal for the generation of ENAs that propagate radially inward. Ring distributions are formed at the shock and in the downstream region. As shown above, these ring distributions could be a strong source of ENAs.

The area between the *Voyager* crossings shows therefore the following important features. First, the TS is closest to the Sun nearer to *V2*. Second, the orientation of the TS surface is perpendicular to the radial direction, i.e., the TS is perpendicular. Ion distributions, in this case ring distributions, gyrating around the interplanetary magnetic field have velocity components that also point toward the Sun. Interstellar neutrals that charge exchange with these ion distributions will very efficiently generate ENAs that have velocities pointed toward the Sun.

5. WHY IS THE ENA EMISSION ONLY WITHIN A LIMITED ANGULAR RANGE?

In the previous sections, we provided evidence that the reflected solar wind could provide enough ENAs within a relatively short line of sight distance. We also explained the role of the interstellar field as a governing factor, the role of the location of the TS with respect to the HP, and the associated gyrating ion distributions. So far, we have not explained why we observe a ribbon-like structure. We propose a simple model, which is based on the global shape of the TS and geometrical considerations. For the sake of simplicity, we assume a coordinate system that has its z-axis aligned with the interstellar field. We also assume here that the TS is symmetric around z. Figure 5 illustrates the situation. The top figure shows the front view of the heliosphere that is enclosed by the interstellar magnetic field. The heliosphere is plane elongated in the z direction, as shown in the second plane, and circular in the x–y plane (first). The bottom two figures show 2D cuts parallel and perpendicular to the interstellar magnetic field. The left-hand figure shows the perpendicular cut and the right-hand figure shows the parallel cut. In this representation, the ribbon should be located in the perpendicular plane to align with the observations. In this plane, we assume that the HP and the TS have a circular shape at least along the front (or upwind) direction and an undetermined shape toward the downwind direction. In the direction parallel to the interstellar field, we use a elliptical function to describe the HP and the TS. The red shaded circles in Figures 6 and 7 indicate a circle around the Sun with a radius r that is the distance from the Sun to the TS. The vector n is the vector normal to the shock surface and the circled dot indicates the orientation of the interstellar magnetic field (out of the plane). Due to the interstellar magnetic field, the HP and the TS are slightly shifted toward the Sun, as shown by the red circle. This shifting is an assumption in this model that is based on results of global MHD simulations showing the impact of the interstellar field on the HP and, to a lesser extend, on the TS (Pogorelov & Matsuda 1998; Ratkiewicz et al. 1998;

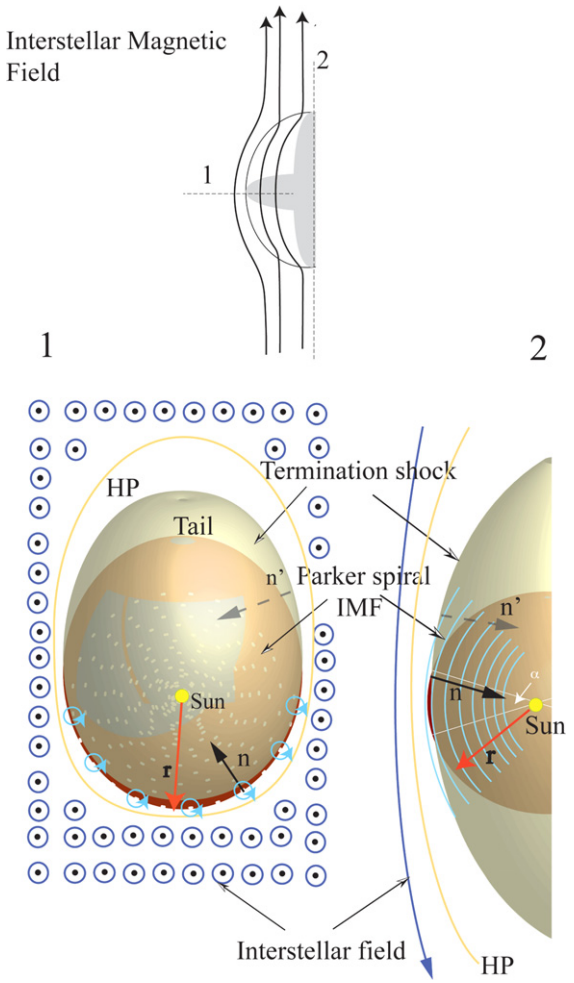

Figure 5. Top panel: schematic representation of the deformation of the heliosphere by the interstellar magnetic field from a head-on point of view. The heliosphere is slightly elongated parallel to the interstellar magnetic field (ISMF). Bottom panels: schematic views perpendicular (1) and parallel (2) to the ISMF. Shown is the HP (thin line), the TS (thick line), and the ISMF. The red circle marks the TS approximated as a sphere with a radial vector r. We also show the vector n, which is normal to the TS. This vector is anti-parallel to the radial vector r in the angular range α.

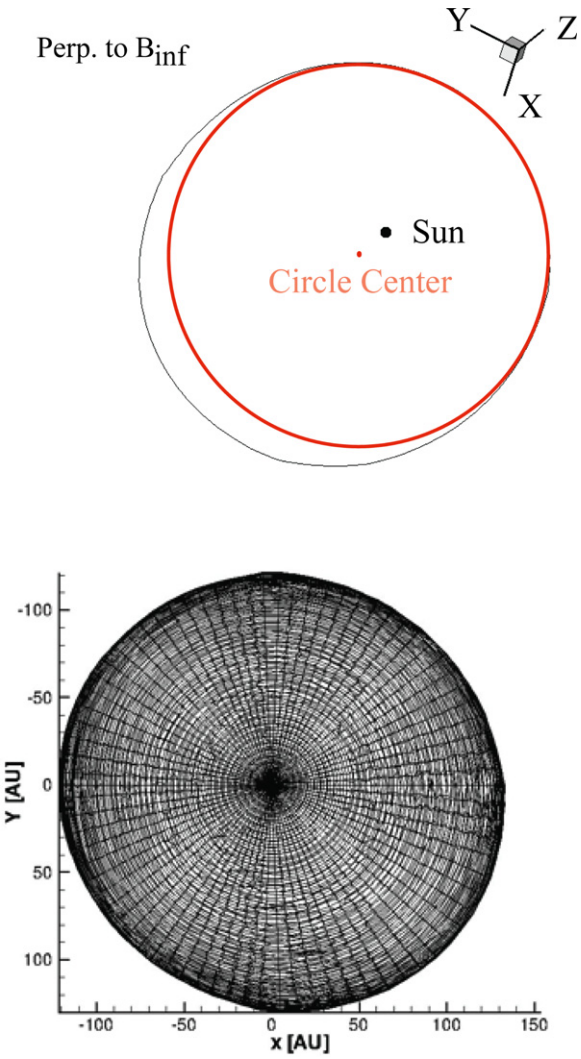

Figure 6. Shape of the termination shock from global MHD simulations. The top panel shows a cut through the TS in a plane perpendicular to the interstellar magnetic field that includes the Sun. In red, we show a fitted circle with its center slightly shifted from the Sun's location. The bottom panel shows a collapsed representation of the global TS, including its flanks.

Izmodenov et al. 2005). Once ENAs are generated by charge exchange with an energetic charged particle, they follow ballistic trajectories unimpeded by any electric or magnetic field. Since the charged particles gyrate perpendicular to the magnetic field at the shock ramp, the preferred emission direction would be along the TS normal. In the plane perpendicular to the interstellar field, the TS is assumed to be almost circular on the front side. In this case, we expect that *IBEX* would detect almost uniform ENA emission because the normal of the TS is anti-parallel to the radial direction. In this simple model, one would therefore expect a uniform ENA emission over an angular range of about 180° degrees. In the plane parallel to the interstellar magnetic field, the angular range would be limited to an angle range α over which the normal vector is equal to the radial vector of the inner circle. Other ENAs will be detected by *IBEX* as long as they enter the entrance system with an angle less than ±3° FWHM.

5.1. MHD Simulations of the Global Shape of the Termination Shock

One assumption used in this model is that the TS is a nearly perpendicular shock in the ribbon area. Global MHD simulations by Pogorelov et al. (2009) confirm this assumption. According to their simulations, the TS is nearly perpendicular, even at higher latitudes. Only in the vicinity of the north or south pole is the shock normal angle (quasi-)parallel. However, the question remains if the approximation of a circle in the plane perpendicular and a parabolic shape in the plane parallel to the interstellar magnetic field in the outer heliosheaths is justified. This question can only be addressed by a comparison with global MHD simulations. In fact, there is no need for the TS to be a full closed circle perpendicular to the interstellar field and a full closed paraboloid parallel to the interstellar field. This situation is probably not realistic because there is a heliotail in the downwind direction. We use this approximation only in the upwind direction and the region that is closest to the TS and from which the strongest ENA emission—the ribbon—is observed. In Figures 6 and 7, we show the result of a global MHD simulation. The top panel of Figure 6 shows a cut through both V_{ISM} and B_{LIC} of the 3D TS. The cut is in the plane of the Sun and perpendicular to the interstellar magnetic field. The red circle shows the shift of the TS (black line) with respect to the Sun. The lower panel shows a collapsed representation

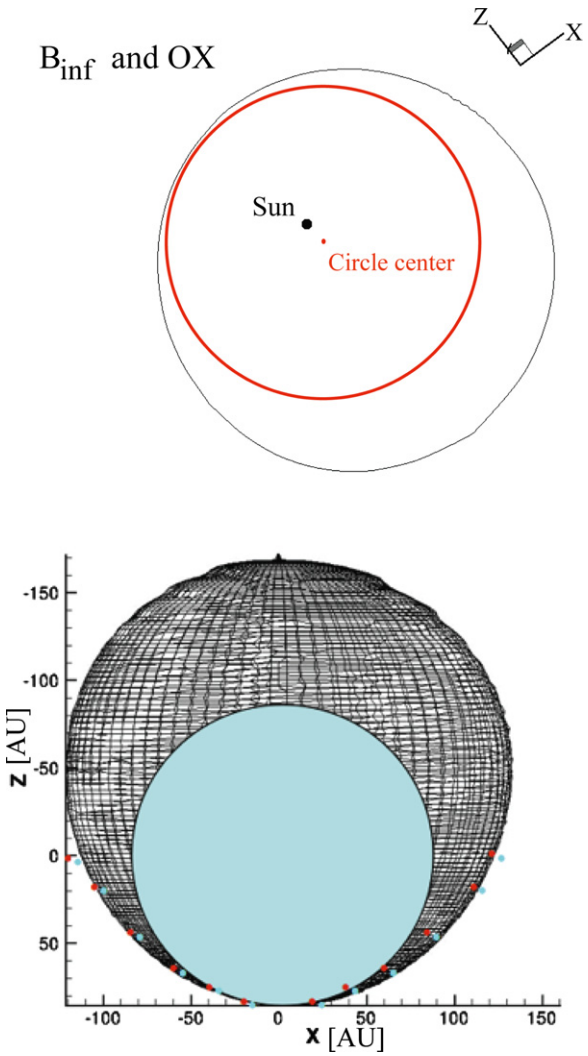

Figure 7. Shape of the termination shock from global MHD simulations. The top panel shows a cut through the TS in a plane parallel to the interstellar magnetic field that includes the Sun. In red, we show a fitted circle with its center slightly shifted from the Sun's location (schematic representation). The bottom panel shows a collapsed representation of the global TS, including its flanks. The light blue shaded area shows a circle with a radius of 84 AU with its center slightly shifted from the Sun's location. The red dots represent a parabola with a radius of 84 AU, whereas the light blue dots represent a fitted parabola of the same radius.

(A color version of this figure is available in the online journal.)

of the TS perpendicular to $\mathbf{B}_{\rm inf}$ (the interstellar magnetic field at infinity). The cut, as well as the collapsed representation, do not resemble a complete circle but a circle can be fit toward the inflow direction. The collapsed figure shows a larger circle than the cuts because the flanks of the TS are included. Figure 7 shows a similar representation as Figure 6. The top panel shows a cut in the plane that is parallel to the interstellar magnetic field; it includes the Sun and the hydrogen deflection plane ("OX" in the figure). A red circle is fit to the nearest point from the Sun to the TS. The bottom panel shows again the collapsed representation. Again, the global shape of the TS is not a circle but a circle can be fit to the closest point to the TS. The red dots represent a parabola with a radius of 84 AU whereas the blue dots show a fitted (slightly shifted) parabola. The blue shaded area represents a circle with a radius of 84 AU that is slightly off center of the Sun's location. These two figures provide a strong indication that both assumptions are in very good agreement with the global MHD simulations. Of course, the exact shape of the TS is unknown because not all possible processes are included in the MHD models. In the next subsection, we will develop an analytic model that uses two basic shapes, a offset sphere and an ellipsoid, to parameterize the TS. We will also show that this parameterized TS can produce a ribbon that can be aligned with $\mathbf{R} \cdot \mathbf{B} = \mathbf{0}$, where $\mathbf{B}$ is the draped interstellar magnetic field. Therefore, this parameterized TS can agree with *IBEX* observations. According to this model, the width, location, and average intensity of the ribbon might therefore be keys to the global shape of the TS. On the other hand, the global shape of the TS may be formed by the interstellar flow and the interstellar magnetic field. Therefore, the interstellar magnetic field is a governing factor in this model because it may determine the global shape of the TS.

5.2. An Analytical Approximation of the Shape of the TS

In this subsection, we present an analytical model that links the global shape of the TS with the IMF. In other words, we parameterize the IMF at the TS and the global shape of the TS. At large heliospheric distances, such as the location of the TS, we approximate the orientation of the IMF as azimuthal about the solar rotation axis. We use a right-handed coordinate system in which the Z-axis is aligned with the solar rotation axis. The X-axis is along the nose direction and the Y-axis is perpendicular to X and Y. More details are provided in Appendix C. In a first step, we approximate the Parker spiral as a sphere that may be slightly offset because of the interstellar flow and the interstellar magnetic field.

An offset sphere, $R(\theta, \phi)$, can be expressed by

$$R = b + \epsilon_1 \cdot \cos(\Theta_1), \tag{7}$$

where $\cos(\Theta)$ is given by

$$\cos(\Theta_1) = \sin(\theta_1)\sin(\theta)\cos(\phi - \phi_1) + \cos(\theta_1)\cos(\theta), \tag{8}$$

where b is the direction of the offset. As discussed in Appendix C, the angles θ_0 and ϕ_0 describe the orientation of the offset in the this coordinate system. θ_0 is the angle between the Z-axis and a vector. ϕ_0 is the angle in the x–y plane. Due to the impact interstellar flow and the interstellar magnetic field, the TS is not a perfect sphere but a combination of a sphere and an ellipsoid that is oriented along the draped interstellar magnetic field. It should be pointed out that this aspect of the model is an assumption. The global MHD simulations may provide an indication that this assumption is reasonable. The tail direction will not be addressed in this paper. As shown is Appendix C, one can parameterize an ellipsoid in a similar fashion:

$$R = b + \epsilon_2 \cdot \cos^2(\Theta_2), \tag{9}$$

where $\epsilon_2 = (a - b)$ and a and b are the major and minor axes of the ellipsoid, respectively. Combining the two basic shapes, an offset sphere combined with an ellipsoid leads to the following expression:

$$R = b + \epsilon_1 \cdot \cos(\Theta_1) + \epsilon_2 \cdot \cos^2(\Theta_2) \tag{10}$$

or

$$R = b[1 + \epsilon_1' \cdot \cos(\Theta_1) + \epsilon_2' \cdot \cos^2(\Theta_2)], \tag{11}$$

where ϵ_1' and ϵ_2' are now normalized to b (see Appendix C).

Now, we determine areas at which the TS is perpendicular. In these areas, the ion distributions do not drift along the magnetic

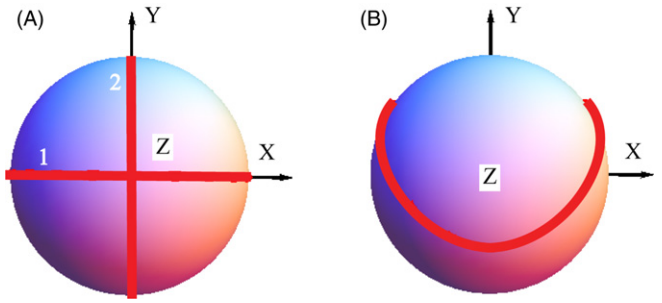

Figure 8. Model shape of the ribbon solving Equation (C5) and Equation (10) or Equation (C12), respectively. Panel (A) shows the two trivial solutions of Equation (C5). The thick red line (1) shows the solution for $\phi = \phi_0$ and line 2 shows the solution $\cos(\Theta) = 0$. Panel (B) shows the non-trivial solution of Equation (C12) in which we combined the ellipsoid with an offset sphere.
(A color version of this figure is available in the online journal.)

field line and the ion distributions gyrate with a 90° pitch angle. We therefore require:

$$\frac{\partial R}{\partial \phi} = -\epsilon_1 \sin(\theta_1)\sin(\theta)\sin(\phi - \phi_1) - 2\epsilon_2 \sin(\theta_2)\sin(\phi)\sin(\theta)\cos(\Theta_2) = 0. \quad (12)$$

This equation depends on the angles θ_1 and ϕ_1 parameterizing the offset of the sphere and θ_2 and ϕ_2 describing the direction of the major axis of the ellipsoid. If the shock normal vector is pointing toward the Sun, ENAs generated in these areas could be detected by *IBEX*. ENAs that charge exchange with ions drifting along the IMF have a lower probability of being detected because *IBEX* can only detect ENAs that enter the entrance system within the field-of-view angle of 7°. For a more detailed discussion of this equation, we refer the reader to Appendix C. The solutions of this equation depend on the overall radius and thus on the semi-principal axis of the ellipsoid, as well as on the location of the sphere with respect to the ellipsoid determined by the angles (θ_1, θ_2 and ϕ_1, ϕ_2). In Figure 8, we show two trivial solutions considering an ellipsoid only (Figure 8(A)) and a non-trivial solution solving Equation (12) or C12, respectively (Figure 8(B)). The red line indicates the location of strictly perpendicular shock conditions at the ellipsoid projected onto a sphere, which would be the location of the ribbon. The red line in Figure 8(B) shows the solution of Equation (C12) for the following set of parameters: $\epsilon_1 = 30.8$, $\epsilon_2 = 17.8$, $\phi_1 = 0, \theta_1 = 0$, and $\Theta_2 = 0.75$ (in radians). Again, the exact location of the line of perpendicular condition—the ribbon—depends on the parameters and, with an optimized parameter set, the ribbon can be reproduced and it does not have to lie on a great circle.

6. DISCUSSION

For the model we presented in this paper, we included *IBEX* and *Voyager* observations, combined results from numerical modeling, and results from the Cluster spacecraft at Earth's bow shock. The main goal of this paper is not to provide a model that reproduces the exact number density of ENAs measured by *IBEX*; the measured numbers are simply used as a guide and a reality check for the model. Instead, the goal of this paper is to demonstrate that a gyrating solar wind and PUIs at the TS and in the heliosheath produce enough ENAs to reproduce the *IBEX* measurements. To determine the ENA flux, we used numbers for the charge exchange cross-section and the density of interstellar hydrogen that are commonly accepted. We have also omitted the loss of ENAs due to charge exchange with solar wind protons, electron impacts, and solar photoionization. However, these processes become important only close to the Sun (<1 AU). Aside from the shape of the TS, only two parameters remaining to determine the ENA flux are the combined flux of solar wind protons and PUIs at the TS and the length of the line of sight integral. In the framework of this model, we distinguish between the distributed ENA flux and the ribbon flux that shows temporal variations and a fine structure, suggesting a compact source region. *IBEX* measurements show that the ribbon flux is roughly a factor of two larger than the distributed flux. We therefore associated half of the total ENA flux with the static, distributed flux. A different ratio could be assumed depending at what flux level the fast variations are visible. Using the Rankine–Hugoniot conditions, a mean pressure of 15×10^{-13} dyn cm^{-2} and a uniformly filled distribution in $V < 2 \cdot V_{sw}$, we determined the total ion distribution far downstream of the TS. With a integral path length of 12–20 AU, the measured distributed *IBEX* ENA flux could be reproduced. This number is in the range of the measured heliosheath thickness but the total pressure downstream of the TS is not very well known. The Rankine–Hugoniot relations assume plasma equilibrium, but the *Voyager* measurements are single-point measurements and it is very difficult to prove that the plasma is in equilibrium. The ribbon ENA flux in this model is associated with ring ion distributions that are very common at the shock and in the downstream region of a supercritical perpendicular shock. As shown above, these ring distributions are a factor of ~10 more efficient at producing ENAs in the plane of the ring than a spherical, thermalized ion distribution. Such a strong source would allow an integral path length of $\lambda = 1$–2 AU and, in turn, fast temporal ENA variations and the fine structure of the ribbon. However, the plasma conditions at the shock ramp and the immediate region downstream of the TS are difficult to determine. Large density and magnetic field variations, as well as unstable ion distributions, are very common. These variations could increase or decrease λ. Another question is the efficiency of the thermalization at the TS. If thermalization processes at the TS are very fast, the ion ring distributions would be destroyed rapidly, reducing the source intensity. A weaker source within a given λ would be explain less intense ENA variations. Therefore, less intense ENA fluctuations could be reproduced by a weaker source and/or a smaller integration path length. How fast the plasma at the TS is thermalized depends on the shock parameters, such as the Mach number, plasma β, and plasma composition. However, these quantities are not very well known. In this model, the ribbon is associated with the global shape of the TS. We approximated the global shape of the TS with two basic 3D shapes: an ellipsoid and an offset sphere. It is plausible that the global shape of the TS is comprised of these two basic shapes in the ram direction. The TS is most likely not a sphere because the interstellar magnetic field and the pressure of the interstellar medium might shift and deform the TS. A strong indication in support of this assumption is provided by global MHD simulations. We then determine the location of ideal perpendicular shock conditions. Under these conditions, the solar wind ions will gyrate perpendicular to the IMF with no parallel drift. These assumptions link the interstellar field with the location of the ribbon because, in this model, the location of the ribbon is determined by global shape of the TS. Although

it can be done, the purpose of this paper is not to reproduce the exact location of the ribbon. The purpose of this paper is rather to suggest a model that can produce a ribbon with a reasonable value for its ENA flux. Hence, the source would be localized and the model would allow slightly faster variations in ENA intensity at the TS than the globally distributed flux that is observed (McComas et al. 2012). The width of the ribbon is not directly addressed in this paper but it may depend on the area in which we can find perpendicular shock conditions. For the smooth TS we have considered, mathematically, this feature is a line, but, due to the local shock structure and its associated turbulence, the TS may widen and form a band or a ribbon. Furthermore, particle scattering may add to the width of the ribbon as well. A detailed analysis of these processes and their association with the ribbon width is beyond the scope of this paper. The global shape of the TS is unknown and this model may be too simple. However, if the ribbon is associated with the global shape of the TS, it may change during a solar cycle. The ribbon may in turn change globally and/or locally. Furthermore, interplanetary disturbances such as GMIRs may lead to local dents in the TS that may lead to very local ENA flux enhancements (hot spots) in the ribbon or in neighboring areas of the ribbon. However, these effects require more detailed investigations and will be the subject of future papers.

7. SUMMARY

We developed a new model for the origin of the ribbon observed by *IBEX* and its temporal and spatial variations. This model is based on thermalized and ring solar wind ion distributions (protons and PUIs), which are located between the shock ramp and the HP. Within this region, these solar wind and PUIs can charge exchange with interstellar neutrals and produce ENAs. In contrast with Heerikhuisen et al. (2010), the source of the ribbon ENAs would be close to the TS and the length of the line of sight integral is much shorter and would allow faster temporal ENA flux variations. The ribbon flux in this model is superimposed on the distributed ENA flux and is associated with ion ring distributions that are located in the shock ramp and in the downstream region of the perpendicular TS. As shown above, the line of sight integral of the distributed ENA flux is much longer (12–20 AU). In fact, this model includes the ribbon and the distributed ENA flux. In this model, ring distributions of solar wind ions gyrating perpendicular to the interplanetary magnetic field are a major contributor to the ribbon flux. ENAs generated by these rings would have velocity vectors in this plane and therefore also in the direction of the Sun. Under perpendicular shock conditions, these ring distributions can generate a significant enhancement in the ENA generation and allow a shorter line of sight integral. The location and width of the ribbon in this model would be determined by the global shape of the TS, which is determined by the interstellar and interplanetary plasma and magnetic field pressure. In this model, the ribbon will be visible along the line at the TS at which we find perpendicular shock conditions. Again, these regions are determined by the global shape of the TS. In an analytical model, we approximated the global shape of the TS by combining an ellipsoid and a sphere. We determined analytically the areas of perpendicular shock conditions and we were able to reproduce a ribbon structure similar to the observed *IBEX* ribbon. Within the framework of this model, one could reproduce the observed ribbon and the distributed flux. Because of the short line of sight integral, fast intensity variations in the ribbon flux would be possible. The ribbon would be a consequence of the global shape of the TS and in turn would directly link the solar wind as a driver for ribbon emissions as a function of latitude (see McComas et al. 2012) and the interstellar plasma and magnetic field with the more static ENA emission, i.e., the globally distributed ENA flux. Furthermore, this model would naturally explain the observed fine structure in the *IBEX* ribbon.

The authors thank E. Roelof for very useful discussions and support for interpreting *Voyager* data. This work was supported by NASA grant NNX09AG62G and the *IBEX* mission, which is part of NASA's Explorer Program.

APPENDIX A

SOLAR WIND DENSITY

There is a large observational uncertainty in the solar wind density at the TS around 1 keV. Measurements made by *V2* (Richardson et al. 2009) show the plasma conditions at higher energies. In order to estimate the ENA flux we assume that the pressure downstream of the TS is given by pressure balance as

$$P = \frac{1}{3} \cdot m \cdot 4 \cdot \pi \int v^4 dv f_0 = \frac{4\pi}{15} \cdot m \cdot (2 \cdot V_{\rm sw})^5 f_0, \quad \text{(A1)}$$

where P is the solar wind pressure. We assume that the distribution function f_0 is uniform between 0–2 $\cdot$ $V_{\rm sw}$. This assumption must satisfy the Rankine–Hugoniot conditions but it should be noted that these assumptions are not valid at the shock transition layer. In this layer, local pressure balance does not apply. The distribution function of the ENAs produced by the interaction of interstellar neutrals with these solar wind ions is then given by

$$f_{\rm ENA} = \lambda \cdot \sigma(E) \cdot n_{\rm H} \cdot f_0. \quad \text{(A2)}$$

In this equation, λ is the line of sight path length, σ is the charge exchange cross-section, $n_{\rm H}$ is the density of interstellar neutrals, and f_0 is the distribution function of the solar wind ions downstream of the TS. Since we assumed pressure balance, the solar wind ion distribution f_0 is presumed to be isotropic.

IBEX measures the differential ENA intensity that can be expressed in terms of the ENA distribution function:

$$J_{\rm ENA} = \frac{v^2}{m} \cdot f_{\rm ENA}. \quad \text{(A3)}$$

If one assumes an average pressure downstream of the TS of $P_{\rm down}$, the only free parameter that is left to determine the observed differential ENA intensity is the line of sight path length λ. For a pressure at the TS of $P_{\rm down} = 15 \times 10^{-13}$ dyn cm^{-2}, a solar wind bulk speed of $V_{\rm sw} = 300$ km s^{-1}, a charge exchange cross-section $\sigma(E) = 3 \times 10^{-15}$ (cm^2) at 1 keV, and a density of the interstellar neutral hydrogen $n_{\rm H} = 0.1$ cm^{-3}, one obtains a simple linear relation between the differential flux and the line of sight path length:

$$J_{\rm ENA} = 12\lambda\,({\rm AU})\,({\rm cm^2\,s\,sr\,keV}). \quad \text{(A4)}$$

IBEX-lo measures a maximum differential ENA flux of $J_{\rm ENA} = 300/[{\rm cm^3\,s\,sr\,keV}]$ in the ribbon structure, which is about two times higher than the ambient ENA flux. For a differential ENA flux of $J_{\rm ENA} = 150/[{\rm cm^3\,s\,sr\,keV}]$, one would need an integration path length of $\lambda = 12$ AU, which is about half of the distance to the HP (Krimigis et al. (2011).

APPENDIX B

ENA DENSITY ENHANCEMENTS BY NON-THERMAL ION DISTRIBUTIONS

In the vicinity of the TS and under perpendicular conditions, a fraction of the solar wind and PUIs is reflected. This region is under perpendicular conditions dominated by gyrating ion distributions gyrating with a 90° pitch angle around the magnetic field. The incoming cold solar wind ion distribution, which is beam-like in velocity space with a main component in the radial direction, will be compressed at, and gradually thermalized after, the shock encounter. Hence, charge exchange can happen at any location at any time and one is left with the question of what is the efficiency of a thermalized and a ring-beam distribution necessary to produce an intense flow of ENAs that can be detected by the *IBEX-lo* sensor. The most intense omni-directional ENA can be produced by a cold omni-directional ion beam that interacts with neutral atoms. A thermalized, in velocity space, isotropic ion distribution with the same number density that interacts by charge exchange with neutral atoms would generate an isotropic ENA distribution in velocity space. A neutral particle detector that only accepts neutrals from a specific direction would detect only a fraction of the produced ENAs. In other words, a ring-beam ion distribution that gyrates perpendicular to the magnetic field would generate a more intense ENA beam perpendicular to the field direction than an isotropic ion distribution of the same number density:

$$f_{0\,\mathrm{ring}} = f_{0\,\mathrm{thermal}} \cdot \gamma, \tag{B1}$$

where γ is an enhancement factor. The differential ENA flux J_{ENA} is directly related to the line of sight path length, which we can write as

$$\lambda_{\mathrm{thermal}} \propto \lambda_{\mathrm{ring}} \cdot \gamma. \tag{B2}$$

This expression reflects the fact that as the intensity of the source ion distribution increases, the integration path length λ decreases. In order to determine the enhancement factor, we consider the area of a circle for a thermal distribution and a segment of a circle for a ring distribution. We obtain

$$\gamma = \frac{2}{x}, \tag{B3}$$

where x is the angular width of the ring in radians. For an angle of 10°, one obtains an enhancement factor of $\gamma \approx 12$. For a ring distribution, which is even more confined, one would obtain a higher factor. This factor will be smaller when thermalization due to wave–particle interactions continues downstream and γ will become 1 if the plasma is fully isotropic.

APPENDIX C

ANALYTIC APPROXIMATION FOR THE SHAPE OF THE TS IN THE NOSE DIRECTION

In this appendix, we approximate the TS in the upwind direction by a combination of two basic shapes: an ellipsoid and a sphere. For the following calculations, we assume a right-handed coordinate system (x, y, z) in which the angle ϕ is in the $X-Y$ plane and θ is the angle with respect to the positive Z axis. A vector in this coordinate system can be written in the following form:

$$\hat{e}R = R(\sin(\theta_0)\cos(\phi_0)\sin(\theta)\cos(\phi) \tag{C1}$$

$$+ \sin(\theta_0)\sin(\phi_0)\sin(\theta)\sin(\phi) \tag{C2}$$

$$+ \cos(\theta_0)\cos(\theta)) \tag{C3}$$

$$= R \cdot \cos(\Theta), \tag{C4}$$

where $\hat{e}$ is a unit vector. The radius of the ellipsoid can be parameterized by

$$R = b + (a - b) \cdot \cos^2(\Theta_2) \tag{C5}$$

or

$$R = b[1 + \epsilon_2' \cdot \cos^2(\Theta_2)], \tag{C6}$$

where $\epsilon_2' = (a - b)/b$.

To find perfect perpendicular shock conditions, we require:

$$\frac{\partial R}{\partial \phi} = 2\epsilon_2' \cos(\Theta_2)\sin(\theta_2)\sin(\theta)(-\sin(\phi - \phi_2)) = 0. \tag{C7}$$

This equation has two trivial solutions: $\phi = \phi_2$ or $\cos(\Theta_2) = 0$.

Similarly, an offset sphere can be expressed by

$$R = b[1 + \epsilon_1 \cdot \cos(\Theta_1))], \tag{C8}$$

where $\cos(\Theta_1)$ is given by

$$\cos(\Theta_1) = \sin(\theta_1)\sin(\theta)\cos(\phi - \phi_1) + \cos(\theta_1)\cos(\theta), \tag{C9}$$

where b' is the average radius. The combination of the two basic shapes leads to

$$R = b[1 + \epsilon_1' \cdot \cos(\Theta_1) + \epsilon_2' \cdot \cos^2(\Theta_2)]. \tag{C10}$$

The factors $\epsilon_1' = \epsilon_1/b$ and $\epsilon_2' = \epsilon_2/b$, $(\epsilon_1', \epsilon_2' < b)$ are associated with the sphere and the ellipse, respectively. For simplicity, we assumed that $\phi_2 = 0$ for the ellipse.

In order to find areas at which the TS is perpendicular, we require:

$$\begin{aligned}\frac{\partial R}{\partial \phi} = & -\epsilon_1 \sin(\theta_1)\sin(\theta)\sin(\phi - \phi_1) \\ & - 2\epsilon_2 \sin(\theta_2)\sin(\phi)\sin(\theta)\cos(\Theta_2) = 0.\end{aligned} \tag{C11}$$

This equation has several trivial solutions. For $\phi = \phi_1$ and $\epsilon_2 = 0$, θ can be any value. In other words, if $\epsilon_2 = 0$ we are left with an offset sphere. If $\epsilon_1 = 0$, the contribution of the offset sphere is 0 and we have an ellipsoid only. For $\epsilon_2 = a - b = 0$, we find a solution for $\phi = \phi_1$ or $\cos(\Theta_2) = 0$; under these conditions, θ can then be arbitrary.

For more non-trivial solutions, this equation can be solved for θ and we obtain:

$$\begin{aligned}\theta = & \cos^{-1}\left[\frac{\cos(\theta_2)}{\sqrt{(1 - \sin^2(\theta_2)\sin^2(\phi)}}\right] \\ & + \cos^{-1}\left[\frac{-\epsilon_1 \sin(\phi - \phi_1)\sin(\theta_1)}{2\epsilon_2 \sin(\theta_2)\sin(\phi)\sqrt{1 - \sin^2(\theta_2)\sin^2(\phi)}}\right].\end{aligned} \tag{C12}$$

REFERENCES

Burgess, D., & Scholer, M. 2007, PhPl, 14, 012108
Burgess, D., Wilkinson, W. P., & Schwartz, S. J. 1989, JGR, 94, 8783
Burlaga, L. F., Ness, N. F., Acuña, M. H., et al. 2005, Sci, 309, 2027
Chalov, S. V., Alexashov, D. B., McComas, D., et al. 2010, ApJL, 716, L99
Cummings, A. C., Stone, E. C., & Steenberg, C. D. 2002, ApJ, 578, 194
Decker, R. B., Krimigis, S. M., Roelof, E. C., et al. 2005, Sci, 309, 2020
Funsten, H. O., Allegrini, F., Bochsler, P., et al. 2009a, SSRv, 146, 75
Funsten, H. O., Allegrini, F., Crew, G. B., et al. 2009b, Sci, 326, 964
Fuselier, S. A., Allegrini, F., Funsten, H. O., et al. 2009, Sci, 326, 962
Gamayunov, K., Zhang, M., & Rassoul, 2010, ApJ, 725, 2251
Gamayunov, V. K., Zhang, M., Pogorelov, N. V., Heerikhuisen, J., & Rassoul, H. K. 2012, ApJ, 757, 74
Gloeckler, G., Möbius, E., Geiss, J., et al. 2004, A&A, 426, 845
Heerikhuisen, J., & Pogorelov, N. V. 2011, ApJ, 738, 9
Heerikhuisen, J., Pogorelov, N. V., Zank, G. P., et al. 2010, ApJL, 708, L126
Izmodenov, V., Alexashov, D., & Myasnikov, A. 2005, A&A, 437, L35
Jokipii, J. R., Giacalone, J., & Kota, J. 2007, P&SS, 55, 2267
Krimigis, A. M., Roelof, E. C., Decker, R. B., & Hill, M. E. 2011, Natur, 474, 359
Krimigis, S. M., Bostrom, C. O., Armstrong, T. P., et al. 1977, SSRv, 21, 329
Liu, Y. C., Lee, M. A., Kucharek, H., & Miao, B. 2007, JGR, 112, A07217
McComas, D. J., Allegrini, F., Bochsler, P., et al. 2009a, SSRv, 146, 11
McComas, D. J., Allegrini, F., Bochsler, P., et al. 2009b, Sci. Express, 326, 959
McComas, D. J., Bzowski, M., Frisch, P., et al. 2010, JGR, 115, A09113
McComas, D. J., Dayeh, M. A., Allegrini, F., et al. 2012, ApJS, 203, 1
Moullard, O., Burgess, D., Horbury, T. S., & Lucek, E. A. 2006, JGR, 111, A09113
Opher, M., Stone, E. C., & Liewer, P. C. 2006, ApJL, 640, L71
Pogorelov, N. V., Heerikhausen, J., Mitchell, J. J., Cairns, I. H., & Zank, G. P. 2009, ApJL, 695, L31
Pogorelov, N. V., & Matsuda, T. 1998, JGR, 103, 237
Pogorelov, N. V., Zank, G. P., & Ogino, T. 2004, ApJ, 614, 1007
Ratkiewicz, R., Barnes, A., Molvik, G. A., et al. 1998, A&A, 335, 363
Ratkiewicz, R., Barnes, A., & Spreiter, J. R. 2000, JGR, 105, 25021
Ratkiewicz, R., Strumik, M., & Grygorczuk, J. 2012, ApJ, 756, 6
Richardson, J. D., Stone, E. C., Kasper, J. C., Belcher, J. W., & Decker, R. B. 2009, GeoRL, 36, L10102
Roelof, E. C., Krimigis, S. M., Mitchell, D. G., et al. 2010, in AIP Conf. Proc. 1302, Implications of Generalized Rankine–Hugoniot Conditions for the PUI Population at the Voyager 2 Termination Shock, ed. J. A. le Roux, V. Florinski, G. P. Zank, & A. J. Coates (Melville, NY: AIP), 133
Schwadron, N. A., Allegrini, F., Bzowski, M., et al. 2011, ApJ, 731, 56
Schwadron, N. A., Bzowski, M., Crew, G. B., et al. 2009, Sci, 326, 966
Stone, E. C., Cummings, A. C., McDonald, F. B., et al. 2005, Sci, 309, 2017
Vasyliunas, V., & Siscoe, G. 1976, JGR, 81, 1247